

Thermodynamic and transport properties of YTe_3 , $LaTe_3$, and $CeTe_3$

N. Ru and I. R. Fisher*

Geballe Laboratory for Advanced Materials and Department of Applied Physics, Stanford University, Stanford, California 94305, USA

(Received 13 September 2005; revised manuscript received 23 November 2005; published 11 January 2006)

Measurements of heat capacity, susceptibility, and electrical resistivity are presented for single crystals of the charge density wave compounds YTe_3 , $LaTe_3$, and $CeTe_3$. The materials are metallic to low temperatures, but have a small density of states due to the charge density wave gapping large portions of the Fermi surface. $CeTe_3$ is found to be a weak Kondo lattice, with an antiferromagnetic ground state and $T_N=2.8$ K. The electrical resistivity of all three compounds is highly anisotropic, confirming the weak dispersion perpendicular to Te planes predicted by band structure calculations.

DOI: [10.1103/PhysRevB.73.033101](https://doi.org/10.1103/PhysRevB.73.033101)

PACS number(s): 71.45.Lr, 72.15.-v, 75.20.Hr

I. INTRODUCTION

The title materials belong to the family of quasi-two-dimensional charge density wave (CDW) compounds RTe_3 , where $R=Y, La-Sm, Gd-Tm$.¹⁻¹⁰ The CDW was first observed for these materials by DiMasi and co-workers² via transmission electron microscopy (TEM). They found superlattice peaks corresponding to a single incommensurate modulation wave vector, with a magnitude $q_{CDW} \approx 2/7$ ($2\pi/a$), varying slightly with R . The incommensurate superstructure was subsequently solved for $R=Ce, Pr, and Nd$ by Malliakas *et al.* using a four-dimensional analysis.³ Angle resolved photo emission spectroscopy (ARPES) experiments on $SmTe_3$ (Ref. 4) and $CeTe_3$ (Refs. 5,6) have confirmed the description of the lattice modulation in terms of a CDW, graphically showing how the electronic structure is gapped for regions of the Fermi surface that are optimally nested. Consistent with the large size of the CDW gap [up to a maximum of 400 meV for $CeTe_3$ (Ref. 5)], the material appears to be deep in the CDW state even at room temperature, and no CDW transitions are observed in the resistivity up to 300 K.^{7,8}

The average (unmodulated) structure of RTe_3 is shown in Fig. 1. The lattice is weakly orthorhombic, belonging to space group $Cmcm$ ⁹ (No. 63), and consists of two structural motifs: nominally square planar Te sheets and corrugated R Te slabs. Note that in the standard space group setting, the b axis is oriented along the long crystal axis, perpendicular to the Te planes. First principle band structure calculations by Laverock *et al.*¹⁰ reveal broad sheets of Fermi surface with very little b -axis dispersion, that principally derive from p_x and p_y orbitals of the planar Te sites. Seen along the b axis, the Fermi surface consists of inner and outer square sheets (both of which are doubled due to the effect of bilayer splitting), large regions of which are nested by a single incommensurate wave vector corresponding to the observed lattice modulation.¹⁰

Given both the large size of the CDW gap and the simplicity of the electronic structure of this material, the RTe_3 family has attracted a growing amount of interest as a model set of compounds to study the effect of incommensurate modulation on electronic structure. However, remarkably little is known about the low-temperature thermodynamic

and transport properties of these materials. In this paper we describe an alternative crystal growth technique for these compounds, and present results of heat capacity, susceptibility, and resistivity measurements for the two nonmagnetic members of the rare-earth series (YTe_3 and $LaTe_3$) and for $CeTe_3$ (specifically chosen since our first ARPES experiments were for this particular compound⁵). We show that the materials have a very low density of states, caused by the CDW gapping a substantial portion of the Fermi surface. We also show that $CeTe_3$ exhibits weak Kondo behavior, implying that there will be some small $4f$ contribution to the Fermi surface at low temperatures for this compound.

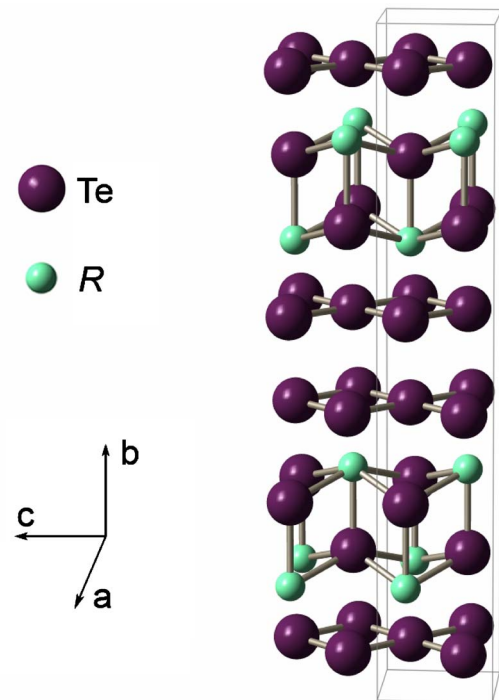


FIG. 1. (Color online) Schematic diagram showing the average crystal structure of RTe_3 ($R=Y, La-Sm, Gd-Tm$). Dashed lines show the unit cell.

II. SAMPLE PREPARATION AND EXPERIMENTAL METHODS

Single crystals were grown via a self-flux technique, similar to our previous report for the related single-layer compounds LaTe_2 and CeTe_2 .¹¹ We favor this technique over the alkali halide flux technique⁷ that has been previously used because it does not introduce other elements to the melt, and produces large crystals with a high degree of structural order. Elements in the molar ratio $R_x\text{Te}_{1-x}$, $x=0.015-0.030$, were put into alumina crucibles and vacuum sealed in quartz tubes. The mixtures were heated to 800–900 °C and slowly cooled over a period of 4 days to end temperatures in the range of 500–600 °C. The remaining melt was decanted in a centrifuge. Resulting gold-colored crystals were malleable, micaceous plates with dimensions of up to $5 \times 0.4 \times 5$ mm, and oriented with the long b axis perpendicular to the plane of the crystal plates. The material is somewhat air sensitive, and crystals must be stored in an oxygen and moisture-free environment. High residual resistance ratios (up to 120) confirm the crystal quality.

The heat capacity of the single-crystal samples was measured using a relaxation time technique in a Quantum Design Physical Property Measurement System (PPMS). Crystals with a mass of approximately 10 mg and flat surfaces were selected for good thermal contact with the sample platform. Data were taken in zero applied field from 1.8 to 300 K.

Magnetization measurements were made using a commercial (Quantum Design MPMS5) SQUID magnetometer. Applied fields of 1000 and 5000 Oe were used to measure the temperature dependence of the low field dc susceptibility (M/H) from 1.8 to 300 K. Data were taken for fields oriented in an arbitrary direction in the ac -plane (i.e., in the plane of the Te sheets).

The electrical resistivity was measured using geometric bars cut and cleaved from the larger as-grown crystals. Electrical contact was initially made using Dupont 4929 silver epoxy directly on to the crystal surface, with typical contact resistances of 10–15 Ω . Subsequent experiments used evaporated gold pads, with improved contact resistances of 2–3 Ω . Resistivity measurements were made using an LR-700 ac resistance bridge operating at 16 Hz. In-plane measurements were made for arbitrary current directions in the ac -plane, using a standard four point contact geometry. The b -axis resistivity was measured using a modified Montgomery¹² geometry, with one current and one voltage contact on the top face of the platelike crystal, and the other voltage and current contacts on the bottom face. Several measurements were made for each compound.

III. RESULTS

Heat capacity data for the two nonmagnetic members of the $R\text{Te}_3$ series ($R=Y$ and La) are shown in Fig. 2. Linear fits to C_p/T vs T^2 were performed from 2.1 to 3.7 K for YTe_3 and 1.9 to 3.7 K for LaTe_3 , avoiding the slight deviation from linearity below 2 K which is presumably associated with a nuclear Schottky anomaly. The resulting estimate for the low- T T^3 coefficient gives Debye temperatures Θ_D of

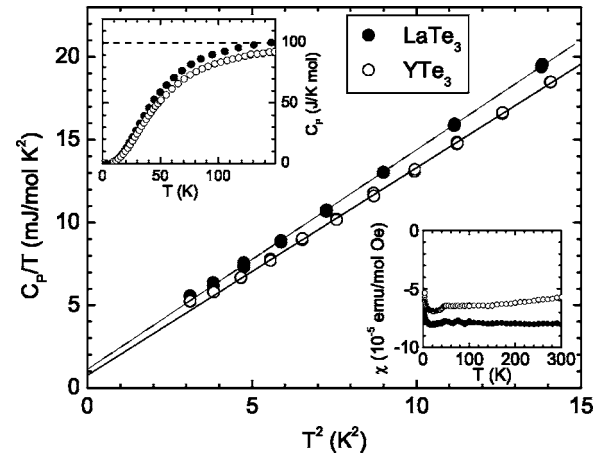


FIG. 2. Low-temperature heat capacity C_p of YTe_3 and LaTe_3 , shown as C_p/T vs T^2 . Straight lines show linear fits as described in the main text. The upper inset shows C_p vs T to 150 K, with the dashed line marking the Dulong-Petit value ($4 \times 3R = 99.7$ J/mol K). The lower inset shows susceptibility of YTe_3 and LaTe_3 for fields oriented in the ac -plane.

183.8 ± 0.5 and 180.4 ± 0.5 K for YTe_3 and LaTe_3 respectively, the small difference due to the different atomic weights of Y and La. The y intercept of the linear fit gives the electronic contribution to the heat capacity, with $\gamma = 0.8$ and 1.1 ± 0.1 mJ/mol K^2 for YTe_3 and LaTe_3 , respectively. Within a free-electron model, these values correspond to densities of states of 0.33 and 0.48 states/eV/f.u., respectively, for the two compounds.

The susceptibility of YTe_3 and LaTe_3 , shown in the lower inset to Fig. 2, is diamagnetic and largely temperature independent. Rough estimates of the Pauli susceptibility give values for the density of states that agree with those found from heat capacity measurements. A weak contribution from magnetic impurities is observed at low temperatures, consistent with the starting purities of the rare-earth elements (99.5%). The small feature at 50 K corresponds to trapped oxygen.

The anisotropic resistivity of LaTe_3 is shown in Fig. 3.

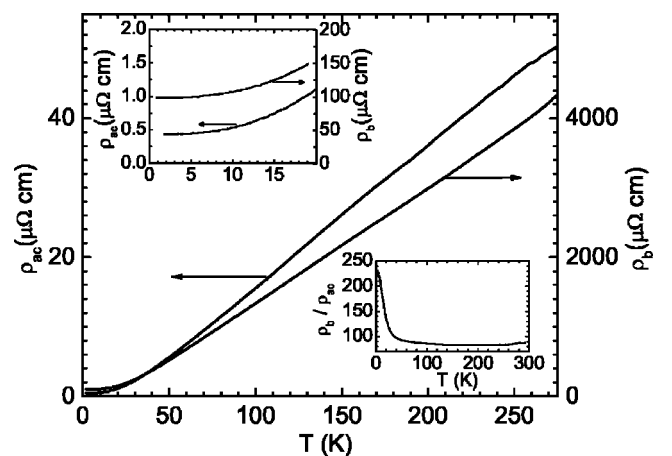


FIG. 3. Representative resistivity data for LaTe_3 , for currents flowing in the ac -plane (left axis) and along the b axis (right axis). Insets show (top) residual resistivity and (bottom) temperature dependence of anisotropy ρ_b/ρ_{ac} .

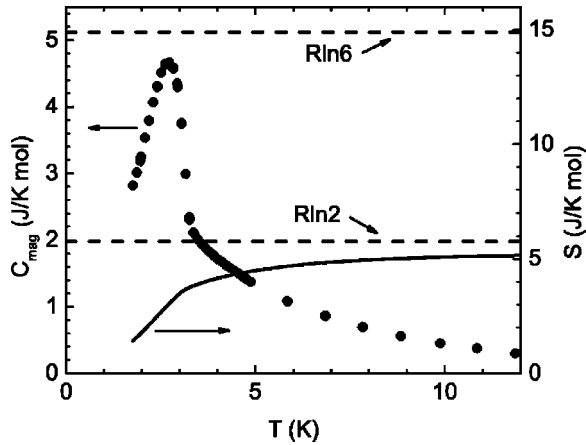


FIG. 4. The magnetic contribution to the heat capacity of CeTe_3 (left axis) and the magnetic entropy (right axis). Dashed lines show $R \ln(2J+1)$ and $R \ln 2$ (right axis).

The material is clearly metallic, due to the presence of significant ungapped portions of the Fermi surface, and the resistivity follows a temperature dependence which has only subtle differences from the Bloch-Grüneisen form. As has been previously noted for SmTe_3 ,⁷ the material has a large anisotropy, confirming the weak b -axis dispersion suggested by band structure calculations.¹⁰ For the crystals that were used for b -axis resistivity measurements, the equivalent isotropic crystals¹² had typical aspect ratios of approximately one-to-one, implying that our estimates of the b -axis resistivity are meaningful. Values of ρ_b/ρ_{ac} (where subscripts refer to the direction in which current is flowing) are approximately 100 above 40 K, rising to over 200 at 1.8 K, a value somewhat smaller than previous estimates by DiMasi and co-workers for SmTe_3 .⁷

The low-field susceptibility of CeTe_3 has been described by Iyeiri *et al.*⁸ Our results broadly corroborate their findings, so we do not reproduce them here. The susceptibility is found to follow a Curie-Weiss behavior, with only modest deviations below 50 K suggestive of CEF splitting of the Hund's rule J multiplet. The effective moment obtained from fits for temperatures above 150 K is $2.4\mu_B$, consistent with the expected value for trivalent cerium. The susceptibility is only mildly anisotropic, with the hard axis corresponding to fields oriented parallel to b . Weiss temperatures extracted from the same fits described above give $\Theta_b = -30$ K and $\Theta_{ac} = 1.6$ K for fields oriented along the b axis and in the ac -plane, respectively, indicating predominantly antiferromagnetic interactions. A kink in the quantity $d\chi T/dT$ (lower inset to Fig. 5) at approximately 3 K indicates a possible transition to an antiferromagnetic ground state. This phase transition is more clearly seen in the heat capacity and resistivity, enabling a better estimate of T_N .

The magnetic contribution to the heat capacity of CeTe_3 C_{mag} estimated by subtracting the measured heat capacity of LaTe_3 , is shown in Fig. 4. A sharp anomaly at 2.8 ± 0.1 K indicates the onset of long-range magnetic order. The magnetic entropy associated with this phase transition (right axis of Fig. 4) rises to almost $R \ln 2 = 5.76$ J/mol K just above T_N , indicating a doublet ground state, as previously proposed by

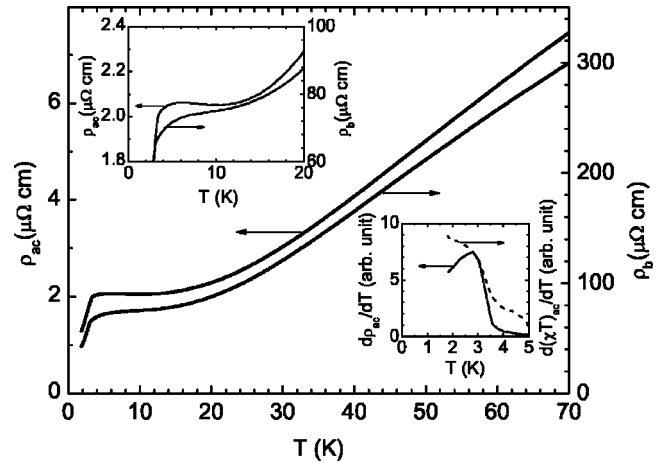


FIG. 5. Representative resistivity data for CeTe_3 for currents flowing in the ac -plane (left axis) and along the b axis (right axis). Insets show (top) low-temperature behavior and (bottom) the Néel transition as seen in $d\rho/dT$ and $d\chi T/dT$.

Iyeiri and co-workers to account for their susceptibility data⁸ and commonly found for Ce in a low point symmetry.

At high temperatures the resistivity of CeTe_3 is similar to that of LaTe_3 , shown in Fig. 3. However, at lower temperatures there is a marked difference, as can be seen in Fig. 5. For currents flowing in the ac -plane, the resistivity has a weak minimum centered at approximately 10 K. As the temperature is reduced from this value the resistivity rises to a broad maximum centered at approximately 6 K, before gradually decreasing in magnitude again. Finally, at 2.8 K there is a sharp drop in the resistivity associated with the loss of spin-disorder scattering at T_N (seen more clearly in the derivative $d\rho/dT$; lower inset to Fig. 5). Similar data for currents flowing in the b -axis direction also show the loss of spin-disorder scattering at T_N but otherwise appear to have a weaker temperature dependence below 10 K, such that the resistivity exhibits more of a change in downward slope than a true upturn.

IV. DISCUSSION

The density of states of YTe_3 and LaTe_3 estimated from our heat capacity measurements are significantly smaller than values calculated for the unmodulated crystal structure [0.8 states/eV/f.u. (Refs. 10,13)], confirming via a bulk measurement that substantial regions of the Fermi surface have been gapped by the CDW modulation. Ungapped portions of the original Fermi surface then contribute the observed metallic properties, with small differences in the measured density of states for the two compounds likely reflecting subtle differences in the nesting features of their respective Fermi surfaces.

In spite of their small density of states, the $R\text{Te}_3$ compounds are very good metals. The residual resistance of LaTe_3 is less than $0.5 \mu\Omega \text{ cm}$, and the residual resistance ratio is over 100. The layered crystal structure contributes a very anisotropic resistivity tensor, characterized by $\rho_b/\rho_{ac} \approx 100$. Below 40 K this quantity rises still further, pre-

sumably reflecting increased scattering for currents flowing in the b -axis direction relative to within the Te planes. Given the layered crystal structure, this effect is possibly associated with elastic scattering from stacking faults in the b -axis direction.

CeTe₃ is antiferromagnetic, with a Néel temperature $T_N=2.8\pm 0.1$ K. Below 10 K the resistivity of CeTe₃ shows a mild upturn, suggestive of weak Kondo behavior. In this case, the broad maximum in the resistivity centered at approximately 6 K is associated with a coherence temperature of the Kondo lattice. ARPES data^{6,14} show a nondispersing feature 0.3 eV below E_F associated with the Ce $4f$ levels, consistent with such a scenario. Given the low value of T_N it is difficult to say whether there is any enhanced electronic contribution to the heat capacity at low temperatures, but the smallness of the resistivity anomaly suggests there will be minimal effect.

It is uncommon to find a Kondo lattice in an incommensurate CDW compound, and the interplay of these two physical effects raises some interesting questions. CDW formation not only reduces the number of electrons available to screen the Ce moment, but also results in a spatially varying local density of states (different for every Ce site for a truly incommensurate modulation), which would in principle be antagonistic to formation of coherence between local screening clouds. Nevertheless, the material is able to accommodate both physical effects, implying that the average density of

states provides the screening, which must be extended over fairly large distances.

V. CONCLUSIONS

In summary, we have described an alternative technique to grow large, high-quality single crystals of the rare-earth tritellurides $R\text{Te}_3$. Our heat capacity and susceptibility measurements for the nonmagnetic members of this series ($R=Y$ and La) indicate that the materials have a very low density of states associated with the small reconstructed Fermi surface in the CDW state. The Ce ion in CeTe₃ is trivalent at high temperatures, but the compound exhibits weak Kondo lattice behavior below approximately 10 K, before ordering to an antiferromagnetic ground state below $T_N=2.8$ K. These data imply that at low temperatures there will be a very small $4f$ contribution to the DOS at the Fermi level for CeTe₃, but that this will not substantially affect the nesting features nor the CDW.

ACKNOWLEDGMENTS

We thank J. Laverock and S. B. Dugdale for providing D.O.S. estimates for the unmodulated crystal structures, and V. Brouet and Z. X. Shen for useful discussions. This work is supported by the DOE, Office of Basic Energy Sciences, under Contract No. DE-AC02-76SF00515. I.R.F. was also supported by the Alfred P. Sloan Foundation.

*Electronic address: irfisher@stanford.edu

¹E. Bucher, K. Andres, F. J. di Salvo, J. P. Maita, A. C. Gossard, A. S. Cooper, and G. W. Hall Jr., Phys. Rev. B **11**, 500 (1975).

²E. DiMasi, M. C. Aronson, J. F. Mansfield, B. Foran, and S. Lee, Phys. Rev. B **52**, 14516 (1995).

³C. Malliakas, S. J. L. Billinge, H. J. Kim, and M. G. Kanatzidis, J. Am. Chem. Soc. **127**, 6510 (2005).

⁴G.-H. Gweon, J. D. Denlinger, J. A. Clack, J. W. Allen, C. G. Olsen, E. D. DiMasi, M. C. Aronson, B. Foran, and S. Lee, Phys. Rev. Lett. **81**, 886 (1998).

⁵V. Brouet, W. L. Yang, X. J. Zhou, Z. Hussain, N. Ru, K. Y. Shin, I. R. Fisher, and Z. X. Shen, Phys. Rev. Lett. **93**, 126405 (2004).

⁶H. Komoda, T. Sato, S. Souma, T. Takahashi, Y. Ito, and K. Suzuki, Phys. Rev. B **70**, 195101 (2004).

⁷E. DiMasi, B. Foran, M. C. Aronson, and S. Lee, Comput. Mater. Sci. **6**, 1867 (1994).

⁸Y. Iyeiri, T. Okumura, C. Michioka, and K. Suzuki, Phys. Rev. B **67**, 144417 (2003).

⁹B. K. Norling, H. Steinfink, Inorg. Chem. **5**, 1488 (1966).

¹⁰J. Laverock, S. B. Dugdale, Zs. Major, M. A. Alam, N. Ru, I. R. Fisher, G. Santi, and E. Bruno, Phys. Rev. B **71**, 085114 (2005).

¹¹K. Y. Shin, V. Brouet, N. Ru, Z. X. Shen, and I. R. Fisher, Phys. Rev. B **72**, 085132 (2005).

¹²H. C. Montgomery, J. Appl. Phys. **42**, 2971 (1971); B. F. Logan, S. O. Rice, and R. F. Wick, *ibid.* **42**, 2975 (1971).

¹³S. B. Dugdale (private communication).

¹⁴V. Brouet and Z.-X. Shen (private communication).